Available online at www.sciencedirect.com
SCIENCE DIRECT®
Journal of Sound and Vibration 285 (2005) 887–903
JOURNAL OF SOUND AND VIBRATION
www.elsevier.com/locate/jsvi

Free vibration analysis of radial pneumatic tires using Beźier functions

L. Jia*, Y. Xu, J. Zhang

School of Mechanical Engineering of Shanghai Jiao Tong University

Received 5 September 2003; received in revised form 31 August 2004; accepted 2 September 2004
Available online 23 December 2004

Abstract

A doubly curved shell model is presented to analyze the free vibration of radial pneumatic tires. The model is based on Reddy type refined shell theory with higher-order shear deformation. Tire geometry and displacement fields are represented by piece-wise Beźier polynomials in orthogonal curvilinear coordinates, and a Ritz method is employed to compute the natural frequencies and mode shapes of pneumatic tires. The results show that this method is more accurate, converging faster and less time-consuming than the first-order shear Shell-FEM. It can also keep the same level of accuracy as that of Solid-FEM. The effects of some physical parameters such as the inflation pressure, tread mass, and ply-angles to the natural frequencies of tires are investigated.

1. Introduction

Research on tire performances has been continuously receiving much attention with the rapid development of the automobile and airplane industries. Various approaches have been developed for the analysis of tire vibration and their dynamic response. These models include the simple mathematical models of a ring on a viscoelastic foundation [1–5], the cord-network model [6], as

*Corresponding author. Present address: Department of Mechanical Engineering, College of Engineering, Michigan State University, 2555 Engineering Building, East Lansing, MI, 48824-1226, USA.
E-mail address: jialipin@egr.msu.edu (L. Jia).

0022-460X/$ - see front matter © 2004 Elsevier Ltd. All rights reserved.
doi:10.1016/j.jsv.2004.09.004

well as the more sophisticated models, such as the membrane model [7], the two-dimension Axisymmetric model [8], the two-dimension thin shell and the thick shell model [9–11], the three-dimension solid model [12]. These efforts are motivated by the need for accurate and efficient model for evaluating new tire designs.

The analysis of tires has unique difficulties due to complex mechanics of the rubber–textile composite, the complex tire contour, and the large deformations. These result in time-consuming and costly computation. Today the simple ring model is still a useful tool for predicting tire responses [13]. Two-dimension shell models have been successfully applied to the deformation and geometry analysis of tires to improve the computational accuracy and efficiency [14,15]. But there is still a lack of accurate and efficient mechanical models needed to reduce the design cycle. This has been recognized by the industry [16].

In recent years, researchers have proposed Beźier functions to represent the displacement fields of a double curved shell in orthogonal curvilinear coordinates. Kumar and Singh [17] used quintic Beźier polynomials for the vibration analysis of non-circular cylindrical shells based on the Ritz method. They found that the Beźier polynomials converged much faster and utilized less computer time than the conventional finite strip method. Singh and Kumar [18] extended this method to the free vibrations of fiber reinforced doubly curved panels and included the higher-order shear deformation theory and the effects of rotary inertia in their analysis. Jia and her co-workers [19] proposed a Rayleigh–Ritz method based on using Beźier polynomials to analyze the static response of pneumatic tires, and developed a semianalytical model to calculate the stress and deformations of tires subjected to uniform inflation pressure. Xu et al. [20] applied the same method to predict road/tire interactions, e.g. the footprint shape and stress distributions of the tire under a vertical load.

The present paper deals with free vibration problems of tires. A new shell model is presented that is based on Reddy's type refined shell theory with higher-order shear deformation in general orthogonal curvilinear coordinates, and the effects of rotary inertia are included. The tire geometry and displacement fields are represented by piece-wise Beźier surface patches, and $C^{(1)}$ continuities are enforced between two adjacent patches. The Rayleigh–Ritz method is employed to compute natural frequencies and mode shapes of a pneumatic tire. The influence of some physical parameters such as pressure, tread mass, and ply-angles on the natural frequencies of tires are evaluated. A study of convergence characteristics of the solution procedures is investigated.

2. Basic formulations

The geometry and coordinate system of a tire shell element are shown in Fig. 1, in which the interior contour surface is regarded as the reference surface. In the orthogonal curvilinear coordinates, s, t and z are meridian, circumference, and thickness directions respectively. u, v, w are the displacement components of reference surface, and ϕ_1, ϕ_2 and ϕ_3 are rotations of the cross-section around the s, t and z coordinates, respectively. Any point within the shell can be located by the two orthogonal curvilinear coordinates (s, t) and a third coordinate z normal to the curved surface. The metric scale factors H_1, H_2 and H_3 [17] of a surface at a distance z from

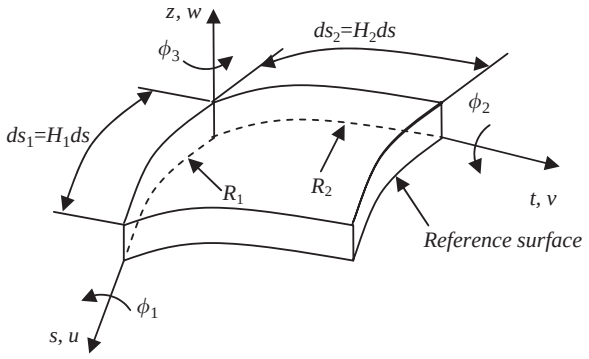

Fig. 1. Curvilinear coordinate system of a tire shell element.

the reference surface can be written as

$$H_\alpha = A_\alpha(1 + z/R_\alpha), \quad \alpha = 1, 2,$$
$$H_3 = 1, \tag{1}$$

in which A_α and R_α are the metric scale factors and principal radii of the reference surface.

The rotation vector around the z-axis ϕ_3 is very small for the shell element. The strain–displacement relations can be obtained by ignoring the higher-order terms and ϕ_3 in the following:

$$\varepsilon_{11} = \frac{1}{1 + (z/R_1)} \left(\frac{1}{A_1} \frac{\partial u_1}{\partial s} + \frac{1}{A_1 A_2} \frac{\partial A_1}{\partial t} u_2 + \frac{u_3}{R_1} \right) + \frac{1}{2} Q_1^2,$$

$$\varepsilon_{22} = \frac{1}{1 + (z/R_2)} \left(\frac{1}{A_2} \frac{\partial u_2}{\partial t} + \frac{1}{A_1 A_2} \frac{\partial A_1}{\partial s} u_1 + \frac{z}{R_3} \right) + \frac{1}{2} Q_2^2,$$

$$\varepsilon_{33} = \frac{\partial u_3}{\partial z}, \tag{2}$$

$$\varepsilon_{12} = \frac{1}{1 + (z/R_1)} \left(\frac{1}{A_1} \frac{\partial u_2}{\partial s} - \frac{1}{A_1 A_2} \frac{\partial A_1}{\partial t} u_1 \right) + \frac{1}{1 + (z/R_2)} \left(\frac{1}{A_1 A_2} \frac{\partial u_2}{\partial t} - \frac{1}{A_1 A_2} \frac{\partial A_2}{\partial s} u_2 \right) + Q_1 Q_2,$$

$$\varepsilon_{13} = \frac{\partial u_1}{\partial z} + Q_1,$$

$$\varepsilon_{23} = \frac{\partial u_2}{\partial z} + Q_2,$$

in which Q_1 and Q_2 are

$$Q_1 = \frac{1}{1 + (z/R_1)} \left(\frac{1}{A_1} \frac{\partial u_3}{\partial s} - \frac{u_1}{R_1} \right), \tag{3}$$

$$Q_2 = \frac{1}{1 + (z/R_2)} \left(\frac{1}{A_2} \frac{\partial u_3}{\partial t} - \frac{u_2}{R_2} \right) \tag{4}$$

$u_1, u_2,$ and u_3 represent the displacement components at a point (s, t, z). The thickness of the shell of a tire is high enough that the transverse shear stress should be considered. Reddy and Liu [21] proposed a higher-order shear deformation shell theory, in which $u_1, u_2,$ and u_3 produce parabolic variation of transverse shear stresses through the thickness and zero at the top and bottom surfaces. They can be written as

$$u_1(s,t,z) = u\left(1+\frac{z}{R_1}\right) + \phi_1\left(z^2 - z^3\,\frac{2+(h/R_1)}{3h+(2h^2/R_2)}\right) - \frac{w_{,1}}{A_1}\,z, \tag{5}$$

$$u_2(s,t,z) = v\left(1+\frac{z}{R_1}\right) + \phi_2\left(z^2 - z^3\,\frac{2+(h/R_1)}{3h+(2h^2/R_2)}\right) - \frac{w_{,2}}{A_2}\,z, \tag{6}$$

$$u_3(s,t,z) = w. \tag{7}$$

The tire is a shell structure laminated of rubber-cord constituents. Cord materials, including nylon, polyester, and steel, etc., consist of unidirectional fibers embedded in a matrix. Material prosperities are often assumed to be transversely isotropic, i.e. $E_2 = E_3$ and $\mu_{12} = \mu_{13}$, with respect to the planes parallel to the 2–3 plane. There are 5 independent constants of each layer, namely $E_1, E_2(= E_3)$, $\mu_{12}(= \mu_{13})$, $G_{12}(G_{13})$, and G_{23}. The constitutive relations of these layers are considered to be

$$\begin{bmatrix}\sigma_{11}\\ \sigma_{22}\\ \tau_{12}\\ \tau_{23}\\ \tau_{13}\end{bmatrix} = \begin{bmatrix} Q_{11} & Q_{12} & 0 & 0 & 0\\ Q_{12} & Q_{22} & 0 & 0 & 0\\ 0 & 0 & Q_{66} & 0 & 0\\ 0 & 0 & 0 & Q_{44} & 0\\ 0 & 0 & 0 & 0 & Q_{55}\end{bmatrix}\begin{bmatrix}\varepsilon_{11}\\ \varepsilon_{22}\\ \varepsilon_{12}\\ \varepsilon_{23}\\ \varepsilon_{13}\end{bmatrix}, \tag{8}$$

where $Q_{11} = E_1/\Delta,\ Q_{22} = E_2/\Delta,\ Q_{12} = V_{21}E_2/\Delta,\ Q_{66} = G_{12},\ Q_{44} = G_{23},\ Q_{55} = G_{13},$ and $\Delta = 1.0 - \mu_{12}\mu_{21}$. Generally, the fibers of the kth individual layer are oriented at an angle θ with respect to the orthogonal curvilinear coordinate s. The constitutive relations of Eq. (8) for that layer must be transformed into shell coordinates, resulting in

$$\begin{bmatrix}\sigma_{11}\\ \sigma_{22}\\ \sigma_{23}\\ \sigma_{13}\\ \sigma_{12}\end{bmatrix} = \begin{bmatrix} \bar{Q}_{11} & \bar{Q}_{12} & 0 & 0 & \bar{Q}_{16}\\ \bar{Q}_{12} & \bar{Q}_{22} & 0 & 0 & \bar{Q}_{26}\\ 0 & 0 & \bar{Q}_{44} & \bar{Q}_{45} & 0\\ 0 & 0 & \bar{Q}_{45} & \bar{Q}_{55} & 0\\ \bar{Q}_{16} & \bar{Q}_{26} & 0 & 0 & \bar{Q}_{66}\end{bmatrix}\begin{bmatrix}\varepsilon_{11}\\ \varepsilon_{22}\\ \varepsilon_{23}\\ \varepsilon_{13}\\ \varepsilon_{12}\end{bmatrix}, \tag{9}$$

in which $\bar{Q}_{ij}$ is shown in Appendix A.

Strain energy of a pneumatic tire can be written as

$$U = \frac{1}{2}\int_A \left(\sum_{n=1}^{N} \int_{h_n} \{\sigma + \sigma_0\}_n^{\mathrm{T}} \{\varepsilon\}_n \, \mathrm{d}z \right) \mathrm{d}S \tag{10}$$

where σ_0 is the initial pre-stress introduced by the inflation pressure, which can be obtained by Jia's model [19], N is the number of layers, h_n is the thickness of the nth layer, A is the surface area of the interior surface, and $\mathrm{d}S = H_1 H_2 \, \mathrm{d}s \, \mathrm{d}t$.

Separating the variables in time and space, the kinetic energy can be written by the following expression:

$$T = \frac{1}{2}\varpi^2 \int_A \sum_{n=1}^{N} \int_{h_n} [\rho_n (u_1^2 + u_2^2 + u_3^2)] \, \mathrm{d}z \, \mathrm{d}S, \tag{11}$$

where ρ_n is the density of the nth layer and ϖ is the frequency parameter.

3. Approximation of the tire geometry

The geometry of the tire is very complex, especially in the radial direction. The radial interior contour curve can be divided into n segments and approximated by a Beźier polynomial for each segment. Fig. 2 shows the geometry and coordinate system of the interior contour curve. The location of any point on the interior curve can be determined with respect to the reference point B and expressed in term of the distance from point B along the curve. The interior contour curve can be parameterized in the following:

$$x = f_1(s), \tag{12}$$

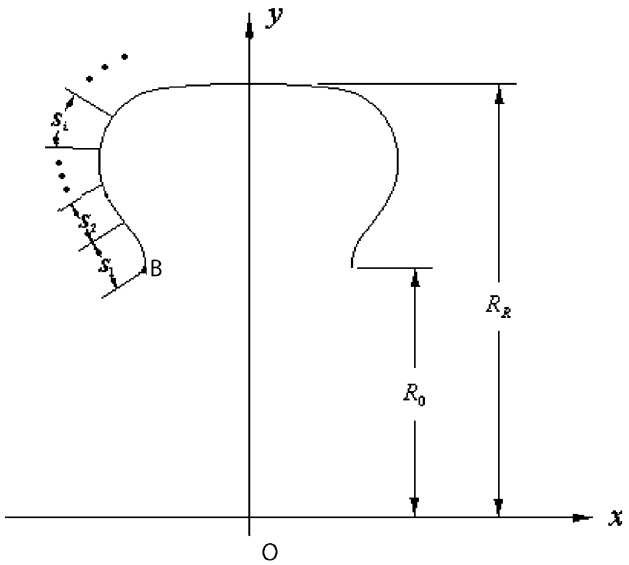

Fig. 2. The divided segments for polynomial approximation of tire contour.

$$y = f_2(s). \tag{13}$$

The interior contour surface can be formed by rotating the curve defined by Eqs. (12) and (13) around the x-axis. The resulting surface is then

$$x = f_1(s), \tag{14}$$

$$y = f_2(s)\cos t, \tag{15}$$

$$z = f_2(s)\sin t, \tag{16}$$

in which t is the rotation angle. The radius vector $\vec{r}$ of any point on the interior contour surface can then be expressed with

$$\vec{r}(s,t) = f_1(s)\vec{i} + f_2(s)\cos t\,\vec{j} + f_2(s)\sin t\,\vec{k}. \tag{17}$$

The principal radii at any point are

$$R_1 = \frac{\left[f'^2_1(s) + f'^2_2(s)\right]^{3/2}}{\left|f''_1(s)f'_2(s) - f'_1(s)f''_2(s)\right|} \tag{18}$$

and

$$R_2 = \frac{f_2(s)\sqrt{f'^2_1(s) + f'^2_2(s)}}{f'_1(s)} = f_2(s)\sqrt{1 + \left[\frac{f'_2(s)}{f'_1(s)}\right]^2}. \tag{19}$$

Define

$$\eta = \frac{s}{s_1} \quad \text{for} \quad 0 \leqslant s \leqslant s_1, \tag{20}$$

$$\eta = \frac{(s - s_1)}{s_2} \quad \text{for} \quad s_1 \leqslant s \leqslant s_1 + s_2,$$

$$\vdots \tag{21}$$

$$\eta = \frac{(s - s_1 - s_2 - \cdots - s_{n-1})}{s_n} \quad \text{for} \quad s_1 + s_2 + \cdots s_{n-1} \leqslant s \leqslant s_1 + s_2 + \cdots s_n, \tag{22}$$

where $s_1, s_2 \ldots$ are the arc lengths of each shell patch along s direction. Any point on the interior curve can be approximated in term of dimensionless variables η:

$$x(\eta) = f_1(\eta) = \sum_{i=1}^{n+1} X_i B_i(\eta), \tag{23}$$

$$y(\eta) = f_2(\eta) = \sum_{i=1}^{n+1} Y_i B_i(\eta), \tag{24}$$

where X_i, Y_i represent $n+1$ vertices of a characteristic polygon and are known as the *control points*. $B_i(\eta)$ is the Bernstein function, which is given as

$$B_i(\eta) = C_i^{n+1}(i,n)\eta^i(1-\eta)^{n-i+1}, \tag{25}$$

in which n denotes the order of the polynomial and the binomial coefficient is given by

$$C_i^{n+1} = \frac{(n+1)!}{(n-i+1)!i!}. \tag{26}$$

4. Rayleigh–Ritz method

The solution procedure is based on a Rayleigh–Ritz method. This requires admissible trial functions for the displacement field. Similar to the geometry approximation of the tire, the displacement fields of the interior contour surface can be approximated by Beźier surface patches. Fig. 3 shows a shell patch bounded by four curvilinear lines. The displacement and rotation of the reference surface (interior contour surface) can be easily approximated by Beźier polynomials in the normalized coordinates η and ξ [17]:

$$\begin{aligned}
u &\approx \sum_{i=1}^{n+1}\sum_{j=1}^{m+1} f_i(\eta)f_j(\xi)P_{U_{ij}},\\
v &\approx \sum_{i=1}^{n+1}\sum_{j=1}^{m+1} f_i(\eta)f_j(\xi)P_{V_{ij}},\\
w &\approx \sum_{i=1}^{n+1}\sum_{j=1}^{m+1} f_i(\eta)f_j(\xi)P_{W_{ij}},\\
\phi_1 &\approx \sum_{i=1}^{n+1}\sum_{j=1}^{m+1} f_i(\eta)f_j(\xi)P_{\phi_{1ij}},\\
\phi_2 &\approx \sum_{i=0}^{n}\sum_{j=0}^{m} f_i(\eta)f_j(\xi)P_{\phi_{2ij}},
\end{aligned} \tag{27}$$

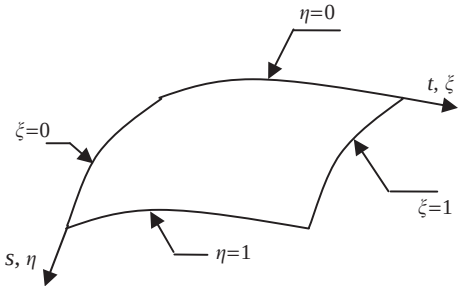

Fig. 3. Normalized and curvilinear coordinates of a shell patch.

where m and n correspond to the degrees of the Beźier polynomials $f_i(\eta)$ and $f_j(\xi)$. $P_{U_{ij}}$, $P_{V_{ij}}$, $P_{W_{ij}}$, $P_{\phi_{1ij}}$, and $P_{\phi_{2ij}}$ denote $(n+1)\times(m+1)$ control points used to represent displacement and rotation.

The total potential energy of the tire is given as

$$\Pi = U - T. \tag{28}$$

Applying Hamilton's variational principle to Eq. (27) by

$$\frac{\partial \Pi}{\partial \{\delta\}} = 0 \tag{29}$$

we can get the following characteristic equation:

$$([K] - \varpi^2[M])\{\delta\} = 0 \tag{30}$$

in which $[K]$ is the stiffness matrix; $[M]$ is the mass matrix and $\{\delta\}^{\mathrm{T}} = \left\{P_{u_{ij}}, P_{v_{ij}}, P_{w_{ij}}, P_{\phi_{1ij}}, P_{\phi_{2ij}} \ldots\right\}$. All these equations are derived by the symbolic software Mathematica 4.0.

5. Numerical examples

Free vibration frequencies of a radial tire P195/60R14 are investigated below. The pneumatic tire is assumed to be fixed on the hub and no vertical load is applied. The effects of damping and temperature on the free vibration are not considered in this research. Fig. 4 illustrates the structure and the material distribution of this tire. It consists of one layer of carcass, two layers of steel belts, two layers of nylon belts and the outer rubber. Carcass, steel belts and nylon belts are

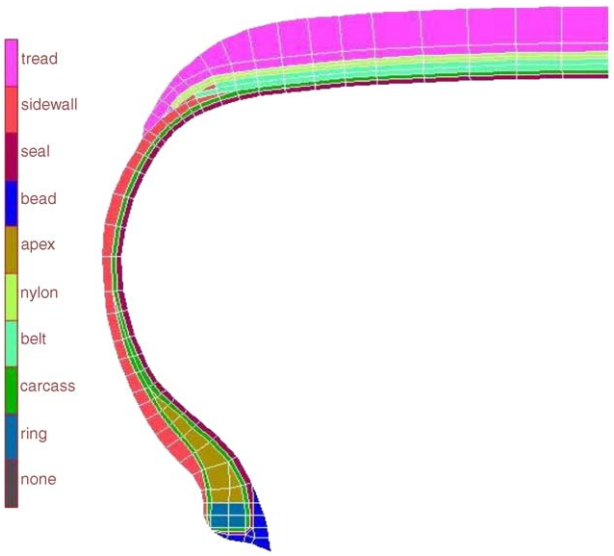

Fig. 4. Configuration and lamination of the P195/60R14 tire.

Table 1
Material properties of the rubber

	E (MPa)	μ	Density (kg/m^3)
Rubber	18	0.49	1.15E03

Table 2
Material properties of cord layers

	E_1 (MPa)	E_2 (MPa)	μ_{12}	G_{12} (MPa)	G_{23} (MPa)	Density (kg/m^3)	Angle (deg)
Nylon belt	809.367	14.75	0.444	4.924	4.924	1.15E03	90
Steel belt	27317.708	12.478	0.46312	4.16	4.16	2.50E03	70
Carcass	1196.15	13.3	0.45976	4.4375	4.4375	1.15E03	0

modeled as orthotropic materials while the rubber is approximated as an elastic material. Material properties of each layer are shown in Tables 1 and 2.

The interior contour curve is divided into 6 segments, each of these could be approximated by second-, third-, fourth-, or fifth-order Beźier curves. From Fig. 5 it can be seen that a second-order Beźier curve cannot accurately describe the curvature around the wire bead. However, a third-order Beźier polynomial provides a good agreement with the original contour. In order to reduce the computational cost, a third-order Beźier polynomial is chosen to approximate the geometry of the interior contour curve.

The mesh for the displacement fields of the interior contour surface is shown in Fig. 6. There are 6 and 12 segments along the radial and circumferential directions, respectively. Third-order of Beźier surface patches are used to approximate the displacement and rotations u, v, w, ϕ_1, ϕ_2.

To verify the effectiveness of this model, two other numerical models, i.e. the first-order shear shell model (Shell-FEM), and the solid model (Solid-FEM) are built by the FEM software Marc to solve the same problem.

Same material properties and geometry as those of the Rayleigh–Ritz model are applied in the Shell-FEM model. The inner surface of the tire is discretized by 20 and 56 4-node thick shell elements along the meridian and circumference directions, respectively, shown in Fig. 7. There are totally 1120 elements and 1140 nodes in the Shell-FEM model. Each of the nodes has five independent degrees of freedom $(u, v, w, \phi_x, \phi_y)$.

Fig. 8 shows the geometry mesh of half of the cross section of the Solid- FEM model. Mesh of the three-dimension structure of the tire is shown in Fig. 9 with 11,232 elements and 12,708 nodes in total. Incompressible Herman solid element is applied in the Solid-FEM model.

6. Results and discussion

6.1. Results for the tire P195/60R14 without patterns

Table 3 and Fig. 10 show the first five natural frequencies and mode shapes of the radial vibration of the tire P195/60R14 obtained by the present Rayleigh–Ritz method, the first-order

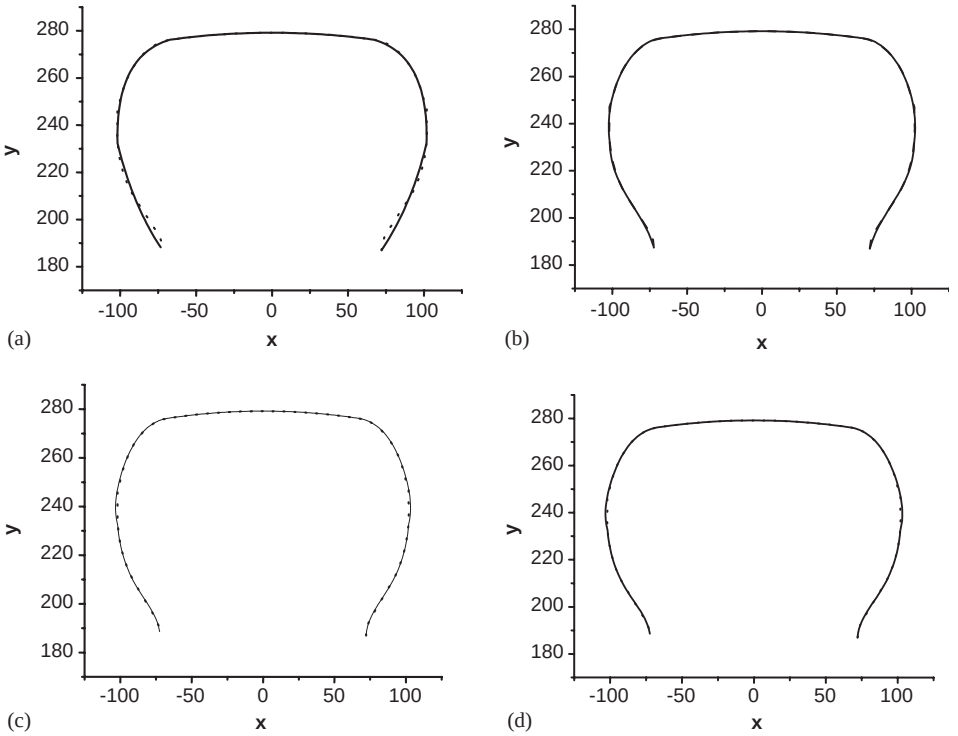

Fig. 5. Inner contour interpolations of the P195/60R14 tire by Bezier polynomials of different orders. ____ the original contour; - - - - - Bezier polynomial; (a) approximation by second-order Bezier polynomial; (b) approximation by third-order Bezier polynomial; (c) approximation by fourth-order Bezier polynomial; (d) approximation by fifth-order Bezier polynomial.

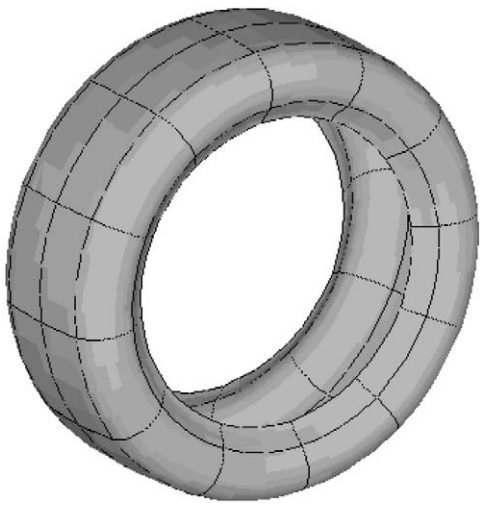

Fig. 6. Piece-wise of inner reference surface of doubly curved shell tire model.

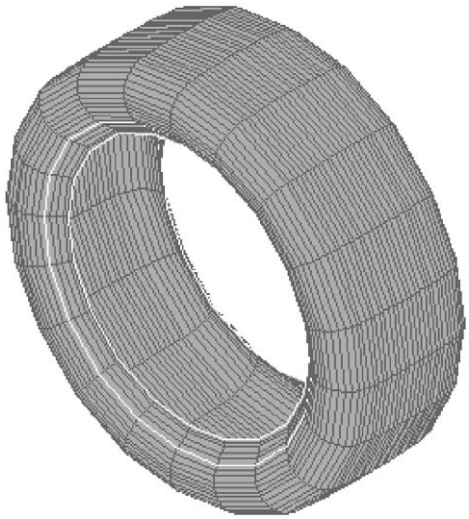

Fig. 7. Mesh of the first-order Shear Shell-FEM model for a whole tire.

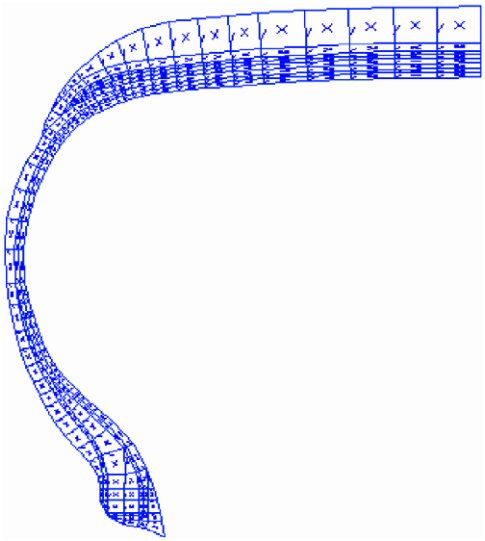

Fig. 8. Discretization for half part of the tire.

shear Shell-FEM, the Solid-FEM, and experiments. The inflation pressure of the tire is 240 kPa. Comparing with the present Rayleigh–Ritz method and the first-order shear Shell-FEM, Solid-FEM can more accurately describe the geometry and displacement fields if the tire is discretized properly. It can be seen from Table 3 that the relative errors of the three numerical methods are large compared with the experimental results. There are some reasons to explain this phenomenon. One is due to the geometry simplification and material approximation. The second reason is that large damping exists at the interface of each layer while the numerical model does not consider this kind of influence.

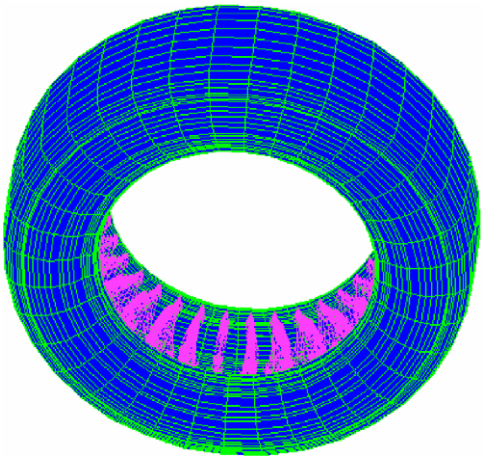

Fig. 9. Solid-FEM model of the tire for numerical analysis.

Table 3
The first five natural frequencies of radial vibrations of the tire P195/ 60R14 under 0.24 MPa inflation pressure

Order	Rayleigh–Ritz		Shell-FEM		Solid-FEM		Experiments [22]
	Natural frequency (Hz)	Relative error (%)	Natural frequency (Hz)	Relative error (%)	Natural frequency (Hz)	Relative error (%)	Natural frequency (Hz)
1	70.2	26.8	66.9	30.0	75.1	21.3	95.5
2	90.8	24.0	79.4	33.5	97.5	18.4	119.5
3	117.2	12.5	108.2	19.4	122.0	8.9	134
4	146.8	5.2	144.5	6.7	150.2	3.1	155
5	187.7	1.4	189.6	2.5	181.7	1.8	185

The computational time used by the three methods is listed in Table 4. It is shown that the present Rayleigh–Ritz method is more accurate than the Shell-FEM. To maintain the same level of accuracy of the natural frequencies, the Solid-FEM takes significantly longer than the proposed method as shown in Table 4. However, the computational speed is faster by the Shell-FEM and the present Rayleigh–Ritz method. Comparing the computational accuracy and efficiency with the three methods, hence, it is effective to use the present Rayleigh–Ritz on the analysis of free vibration of tires.

6.2. *Parametric study*

The effect of three main parameters on the free vibration of tires is investigated by the present Rayleigh–Ritz method.

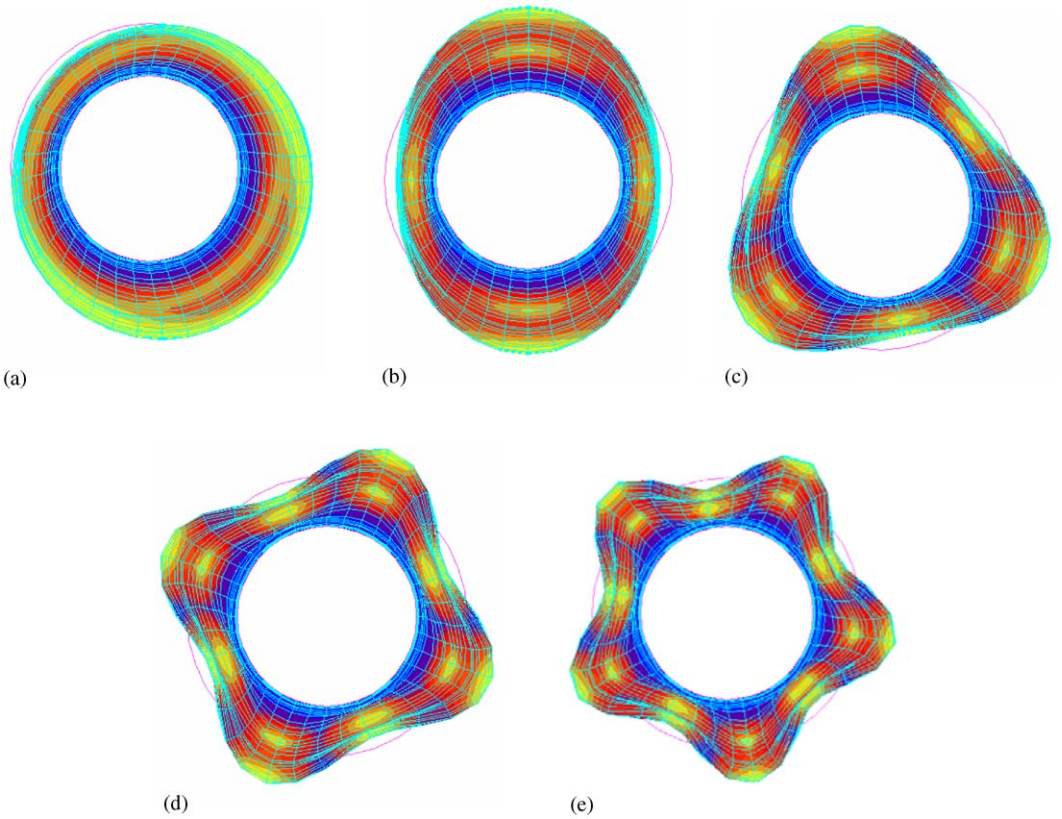

Fig. 10. Mode shapes of radial vibrations of the tire P195/60R14 under the pressure of 240 kPa using the Rayleigh–Ritz method (a) Mode at the 1st natural frequency 70.2 Hz; (b) Mode at the 2nd natural frequency 90.8 Hz; (c) Mode at the 3rd natural frequency 117.2 Hz; (d) Mode at the 4th natural frequency 146.8 Hz; (e) Mode at the 5th natural frequency 187.7 Hz

Table 4
Computational time for the analysis of free vibrations of the tire P195/60R14

	Rayleigh–Ritz method	Shell-FEM	Solid-FEM
Computer type	PIV 1.2 GHz	PIV 1.2 GHz	Workstation
Time (h)	3	3.5	20

6.2.1. *Effect of inflation pressures*

Natural frequencies of free radial vibration of the tire P195/60R14 are calculated by the present Rayleigh–Ritz method under four different inflation pressures, such as 80, 160, 240, and 320 kPa. The inflation pressure directly influences the initial pre-stress and changes the stiffness of the tire. It can be seen from Table 5 that the natural frequencies increase with the higher inflation pressures.

Table 5
The first five natural frequencies of radial vibrations of the tire P195/60R14 under different pneumatic pressure

Order	Natural frequencies (Hz)			
	$P = 80$ (kPa)	$P = 160$ (kPa)	$P = 240$ (kPa)	$P = 320$ (kPa)
1	57.2	63.2	70.2	75.5
2	66.1	81.3	90.8	105.4
3	85.2	101.6	117.2	128.3
4	110.2	127.4	146.8	156.2
5	146.9	168.2	187.7	190.5

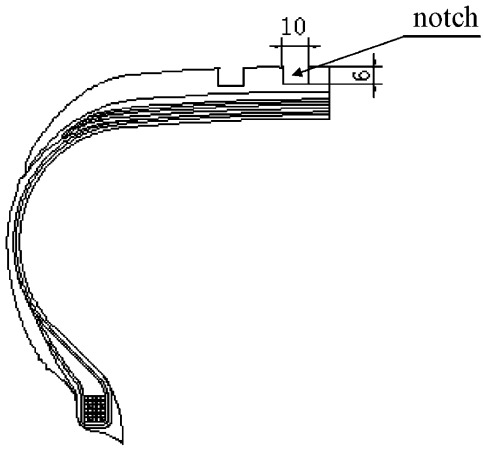

Fig. 11. P195/60R14 tire with patterns.

6.2.2. *Effect of tread patterns*

Tread patterns can increase the friction between the tire and the road and improve the characteristics of driving, rolling resistance, braking, and cornering. The above discussions focus on the tire without patterns. The effect of tread patterns is investigated here. Four shallow circumferential notches are grooved on the tread shown in Fig. 11. Under the inflation pressure 240 kPa, the natural frequencies of two different tires with and without patterns are studied by the present Rayleigh–Ritz method. It is shown in Table 6 that patterns on the tread increase the natural frequencies of the tire.

6.2.3. *Effect of the ply-angles of the steel belts*

Steel belts are the main force-bearing parts in the radial tire. Two layers of steel belts are laminated in different directions. The angle between the orientation of the belt and meridian direction is defined as a ply-angle. Generally the ply-angles of steel belts are between $\pm 60^\circ \sim \pm 70^\circ$. The influence of the ply-angles on the natural frequencies is investigated by the Rayleigh–Ritz method under 240 kPa inflation pressure. From Table 7 it can be seen that the

Table 6
Influence of pattern on the natural frequencies of radial vibrations of the P195/60R14 tire

	1 (Hz)	2 (Hz)	3 (Hz)	4 (Hz)	5 (Hz)
Without patterns	70.2	90.8	117.2	146.8	187.7
With patterns	73.2	108.3	136.5	180.6	213.2

Table 7
Influence of angle of steel belt on natural frequencies of radial vibrations of the tire

Ply angles of steel belts	$\pm 60^\circ$	$\pm 62^\circ$	$\pm 64^\circ$	$\pm 66^\circ$	$\pm 68^\circ$	$\pm 70^\circ$
1st natural frequencies (Hz)	68.9	69.1	69.2	69.7	69.8	70.2

Table 8
Influence of number of patches on the first natural frequency of radial vibrations of the tire

Rayleigh–Ritz method			Shell-FEM		
Number of patches in the circumference direction	Total patches	Frequency (Hz)	Number of elements in the circumference direction	Total elements	Frequency (Hz)
4	24	79.7	14	560	69.4
6	36	72.9	18	720	67.5
8	48	71.2	20	800	67.4
10	60	70.2	26	1040	66. 9
12	72	70.2	28	1120	66. 9

larger the ply-angles, the higher the first natural frequency. However, influence of the ply-angles is not as strong as that of inflation pressures and tread patterns.

6.3. Convergence analysis

To illustrate the computational capability and the effectiveness of the present Rayleigh–Ritz method over the traditional finite element method, a series of numerical solutions for the first natural frequency of the tire P195/60R14 are made. The displacement fields of the cross section are divided into six segments in the Rayleigh–Ritz method and 40 elements in the Shell-FEM. The number of patches along the circumference direction is changed in the two methods. It is shown in Table 8 that the present Rayleigh–Ritz method can converge to the final results when the circumference direction of the tire is divided to 10 patches. For the same problem, however, the first-order shear Shell-FEM model needs 1040 elements to converge. The results show that the Rayleigh–Ritz method converges faster, has less degrees of freedom and uses less computational time than the first shear Shell-FEM model.

7. Conclusion

An efficient numerical approach is presented to predict the vibration frequencies of a radial tire. Beźier polynomials for the displacement fields are used as the trial functions of the Ritz procedure. It is demonstrated that the present approach is accurate and effective for computing vibrations of tires. When compared with the methods of three-dimensional Solid-FEM and Shell-FEM, the present approach can save much CPU time because of the fewer variables in use. From the numerical solutions with different inflation pressures, tread mass, and ply-angles, it is shown that these physical parameters have much influence to the vibrations of tires. Structure designs of tires can be guided by the present analysis. The present method will be further applied to the analysis of footprint of the tire/road interface and dynamic problems of tires.

Acknowledgements

L. Jia wishes to thank professor Youming Long and Jianmin Ge of Shanghai Tire and Rubber Group Co. for the technique support on experiment and Professor Andre Benard at the Department of Mechanical Engineering in Michigan State University for some important review comments.

The financial support by under Contract No. 59675027 and technical assistance from National Key Laboratory for Automotive Dynamic Simulation, Jilin University of Technology are gratefully appreciated.

Appendix A

$$\bar{Q}_{11} = Q_{11}\cos^4\theta + 2(Q_{12} + 2Q_{66})\sin^2\theta\cos^2\theta + Q_{22}\sin^4\theta, \tag{A.1}$$

$$\bar{Q}_{12} = (Q_{11} + Q_{22} - 4Q_{66})\sin^2\theta\cos^2\theta + Q_{12}(\sin^4\theta + \cos^4\theta), \tag{A.2}$$

$$\bar{Q}_{16} = (Q_{11} - Q_{12} - 2Q_{66})\sin^2\theta\cos^3\theta + (Q_{12} - Q_{22} + 2Q_{66})\sin^3\theta\cos\theta, \tag{A.3}$$

$$\bar{Q}_{22} = Q_{11}\sin^4\theta + 2(Q_{12} + 2Q_{66})\sin^2\theta\cos^2\theta + Q_{22}\cos^4\theta, \tag{A.4}$$

$$\bar{Q}_{26} = (Q_{11} - Q_{12} - 2Q_{66})\sin^3\theta\cos\theta + (Q_{12} - Q_{22} + 2Q_{66})\sin\theta\cos^3\theta, \tag{A.5}$$

$$\bar{Q}_{66} = (Q_{11} + Q_{22} - 2Q_{12} - 2Q_{66})\sin^2\theta\cos^2\theta + Q_{66}(\sin^4\theta + \cos^4\theta), \tag{A.6}$$

$$\bar{Q}_{44} = Q_{44}\cos^2\theta + Q_{55}\sin^2\theta, \tag{A.7}$$

$$\bar{Q}_{55} = Q_{44}\sin^2\theta + Q_{55}\cos^2\theta, \tag{A.8}$$

$$\bar{Q}_{45} = (-Q_{44} + Q_{55})\sin\theta\cos\theta. \tag{A.9}$$

Reference

[1] K. Yamagishi, The circumferential contact problem for the belted radial tire, *Computers & Structures* 20 (1–3) (1985) 517–533.

[2] L.E. Kung, W. Soedel, T.Y. Yang, Free vibration of a pneumatic tire–wheel unit using a ring on elastic foundation and a finite element model, *Journal of Sound and Vibration* 107 (2) (1986) 181–194.

[3] S.C. Huang, W. Soedel, Response of rotating rings to harmonic and periodic loading and comparison with the inverted problem, *Journal of Sound and Vibration* 118 (1987) 253–270.

[4] S.C. Huang, C.K. Su, In-plane dynamics of tires on the road based on an experimentally verified rolling ring model, *Vehicle System Dynamics* 21 (1992) 247–267.

[5] C.R. Dohrmann, Dynamics of a tire–wheel–suspension assembly, *Journal of Sound and Vibration* 210 (5) (1998) 627–642.

[6] F. Frank, W. Hofferberth, Mechanics of the pneumatic tire, *Rubber Chemical Technology* 56 (1983) 372–389.

[7] W. Flugge, S.C. Chou, Large deformation theory of shells of revolution, *ASME Journal of Application Mechanical* 34 (1967) 56–58.

[8] H. Kaga, K. Okamoto, Y. Toxawa, Internal stress analysis of the tire under vertical loads using finite element method, *Tire Science and Technology* 5 (1977) 102–118.

[9] G.M. Kulikov, Computational models for multilayered composite shells with application to tires, *Tire Science and Technology, TSTCA* 24 (1) (1996) 11–38.

[10] A.K. Noor, J.A. Tanner, J.M. Peters, Reduced basis technique for evaluating sensitivity derivatives of the nonlinear response of the space shuttle orbiter nose-gear tire, *Tire Science and Technology, TSTCA* 21 (4) (1993) 232–259.

[11] L.E. Kung, W. Soedel, T.Y. Yang, Free vibration of a pneumatic tire–wheel unit using a ring on elastic foundation and a finite element model, *Journal of Sound and Vibration* 107 (2) (1986) 181–194.

[12] J.P. Jeusette, M. Theves, Finite element analysis of tire/rim interface forces under braking and cornering loads, *Tire Science and Technology* 20 (2) (1992) 83–105.

[13] G. Mastinu, S. Gaiazzi, F. Montanaro, D. Pirola, A physical tyre model for steady- and transient-state, in: F. Boehm, H.P. Willumeit (Eds.), *Tyre Models for Vehicle Dynamic Analysis*, Vol. 27, Feb. Supplement to Vehicle System Dynamics, Berlin, 1997, pp. 2–21.

[14] A.K. Noor, C.M. Andersen, J.A. Tanner, Exploiting symmetries in the modelling and analysis of tires, *Computer Methods in Application. Mechanical Engineering* 63 (1987) 37–81.

[15] A.K. Noor, K.O. Kim, J.A. Tanner, Analysis of aircraft tires via semianalytic finite element, *Finite Elements in Analysis and Design* 6 (1990) 217–233.

[16] A.K. Noor, J.A. Tanner, Advances and trends in the development of computational models for tires, *Computers & Structures* 20 (1–3) (1985) 517–533.

[17] V. Kumar, A.V. Singh, Geometrically non-linear dynamic analysis of laminated shells using Beźier functions, *International Journal of Non-Linear Mechanics* 32 (3) (1997) 425–442.

[18] A.V. Singh, V. Kumar, On free vibration of fiber reinforce doubly curved panels, Part 1: formulation/convergence study, *Journal of Vibration and Acoustics* 120 (1998) 287–294.

[19] L. Jia, J. Zhang, Y. Xu, Nonlinear analysis of pneumatic radial tires via piece-wise Rayleigh–Ritz technique, *International Journal of Vehicle Design* 35 (4) (2004) 317–330.

[20] Y. Xu, L. Jia, J. Zhang, Modelling tire/road contact using piecewise Ritz procedure, *Journal of Terramechanics*, in press.

[21] J.N. Reddy, C.F. Liu, A higher-order shear deformation theory of laminated elastic shells, *International Journal of Engineering Science* 23 (3) (1985) 319–330.

[22] J. Ge, Z. Wang, D. Mao, Application of tire experimental modal in the tire structure design, *The 20th Annual Meeting and Conference on tire Science and Technology*, Akron, Ohio, September 2001.